ARTICLES

Journal of Semiconductors
(2021) 42, 092901
doi: 10.1088/1674-4926/42/9/092901

Coupled-ridge waveguide quantum cascade laser array lasing at λ ~ 5 μm

Pengchang Yang[1, 2], Jinchuan Zhang[2, †], Zenghui Gu[2, 3], Chuanwei Liu[2, 3], Yue Zhao[2, 3], Fengmin Cheng[2], Shenqiang Zhai[2], Ning Zhuo[2], Junqi Liu[2, 3], Lijun Wang[2, 3], Shuman Liu[2, 3], and Fengqi Liu[2, 3, †]

[1]School of Microelectronics, University of Chinese Academy of Sciences, Beijing 100049, China

[2]Key Laboratory of Semiconductor Materials Science, Institute of Semiconductors, Chinese Academy of Sciences, Beijing Key Laboratory of Low Dimensional Semiconductor Materials and Devices, Beijing 100083, China

[3]School of Materials Science and Optoelectronics Engineering, University of Chinese Academy of Sciences, Beijing 100049, China

Abstract: In this work, we demonstrated high-power quantum cascade laser (QCL) arrays lasing at λ ~ 5 μm by employing an optimized coupled-ridge waveguide (CRW) structure. Five-element QCL arrays were simulated and fabricated through a two-step etching method to extend the CRW structure to a mid-wave infrared regime. A lateral far-field with the main peak near a diffraction-limited intensity curve of about 10° was observed by properly designing a geometric shape of the ridges and interspaces. By introducing a buried 2nd-order distributed feedback (DFB) grating, substrate emission with a radiation power above 1 W at 25 °C is achieved. Single longitudinal mode operation is obtained by changing the temperature of the heatsink with a good linear wavelength tuning coefficient of –0.2 cm^{-1}/K.

Key words: quantum cascade laser array; coupled-ridge waveguide; mid-infrared

Citation: P C Yang, J C Zhang, Z H Gu, C W Liu, Y Zhao, F M Cheng, S Q Zhai, N Zhuo, J Q Liu, L J Wang, S M Liu, and F Q Liu, Coupled-ridge waveguide quantum cascade laser array lasing at λ ~ 5 μm[J]. *J. Semicond.*, 2021, 42(9), 092901. http://doi.org/10.1088/1674-4926/42/9/092901

1. Introduction

Quantum cascade lasers (QCLs) have been intensely researched in recent years for narrow line-width and high power mid-infrared (MIR) emissions excited by the desperate need of applications, for instance remote gas-sensing, free-space optical communication and high-resolution spectroscopy[1–3]. The narrow ridge width is an indispensable condition for QCL high-power continuous wave (CW) operation at room temperature, as heat dissipation of the device is always a huge challenge. On the other hand, very high peak power is also required in some applications, the peak power of QCLs can be scaled up by increasing the laser gain volume, containing a straightforward way in which we could increase the ridge width, thus increasing the laser gain volume. But simply increasing the ridge width would result in poor beam quality arising from the high-order transverse mode[4]. The spectral and far-field properties of broad area QCLs can be enhanced by the photonic crystal distributed feedback (DFB) mechanism, master-oscillator power-amplifiers, tilted facet lasers, and so on[5–8]. Compared with single-ridged devices, coherent QCL arrays show a great advantage in increasing the peak power and improving the beam quality. Phase locking of QCL arrays has been demonstrated through evanescent waves, resonant leaky-waves, Talbot cavity and Y-junction tree-array coupling[9–14]. In recent years, Liu *et al.* demonstrated a QCL based on a coupled-ridge waveguide (CRW) structure with an emitting wavelength of 7.3 μm[15, 16]. Through carefully designing the CRW structure, the ridge area mainly confined the light field while the coupling ridge region has a gain that exceeded the loss. However, the CRW structure was more suitable for long-wave infrared QCL devices and applying this structure to mid-infrared QCL devices was still a challenge due to the high modal loss and the weak coupling strength among the array elements.

In this paper, we demonstrated high peak power substrate-emitting DFB QCL arrays lasing at λ ~ 5 μm by employing an optimized CRW structure. Five-element QCL arrays were simulated and fabricated through a two-step etching method to extend the CRW structure to a mid-infrared. By introducing a buried 2nd-order DFB grating, the devices could work at a stable single longitudinal mode with a linear tuning coefficient of –0.2 cm^{-1}/K. Lateral far-field with the main peak near the diffraction-limited intensity curve of about 10.7° was observed in a ridge-width direction even at full power. The peak output power from the substrate surpassed 1 W at 25 °C. The main-lobed far-field distribution and high output power of these devices make them very essential in real applications.

2. Simulation and fabrication

A double-phonon resonant design was introduced into the active region of this device with an emitting wavelength of 5 μm. The whole wafer was co-grown by solid-source molecular beam epitaxy (MBE) and metal organic vapor phase epitaxy (MOVPE) on an n-InP substrate (Si, 2×10^{17} cm^{-3}). The active region and InGaAs confined layers were grown by MBE

Correspondence to: J C Zhang, zhangjinchuan@semi.ac.cn; F Q Liu, fqliu@semi.ac.cn

Received 9 FEBRUARY 2021; Revised 8 APRIL 2021.

and the InP cladding was grown by MOVPE. Along the epitaxial layers sequence, the InP bottom cladding layer (5 μm, Si, 2.2 × 10^{16} cm^{-3}), InGaAs confined layer (300 nm, Si, 2 × 10^{16} cm^{-3}), active region (40-stages $In_{0.6}Ga_{0.4}As/In_{0.4}Al_{0.6}As$ superlattice with a strain-compensated design and a total thickness of ~2 μm), InGaAs confined layer (300 nm, Si, 2 × 10^{16} cm^{-3}), InP upper cladding layer (3 μm, Si, 2.2 × 10^{16} cm^{-3}), InP gradually doped layer (250 nm, Si, 2 × 10^{17} to 5 × 10^{17} cm^{-3}) and InP highly doped contact layer (500 nm, Si, 5.5 × 10^{18} cm^{-3}) was grown respectively.

Before fabrication, simulation was conducted with COMSOL to select the optimal parameters of the CRW structure. Based on our earlier research, the mode selection of the array was mainly related to the modal waveguide loss[15]. Fig. 1(a) showed the near-field distribution of the fundamental supermode and high-order supermode. The loss difference of the modal waveguide between the high-order supermode and the fundamental supermode was simulated as the variable of the ridge width W with a constant array period S of 9 μm, as is shown in Fig. 1(b). The grating etching depth D was also fixed at 3.5 μm. In order to ensure the fundamental mode lasing, the ridge width should not be too wide, often requiring less than 8 μm for the laser with a wavelength of 5 μm. If the ridge width is too small (such as less than 5 μm), the absorption loss of silicon oxide will increase. The maximal loss difference was observed at $W = 7$ μm and the loss difference was about 0.0035 cm^{-1}. Besides, the dependence of loss difference of the modal waveguide between the high-order and fundamental supermode on etching depth with a fixed wavelength and period of array S as shown in Fig. 1(c). We observed that the loss difference did not convert positively until the etching depth reached 3.5 μm, which would promote the fundamental supermode in domination. Whereas the actual etching depth was limited by the thickness of the InP top cladding layer and the anisotropy of the etching method. Therefore, we proposed a two-step etching method to get high loss difference for fundamental supermode operation. What's more, the rationality of setting array period to 9 μm was verified, as is shown in Fig. 1(d). Since all the ridges are identical emitters, the far-field pattern will result from the ridge array diffraction. In order to limit the major far-field lobes to one, it is necessary to shorten the interval according to the equation:

$$S \sin\theta = \pm (k + \delta/2\pi)\lambda,$$

where S is the period of the ridges, θ is the diffraction angle, and δ is the phase shift between adjacent emitters. A smaller interval between the ridges would also lead to a negative loss difference with a fixed ridges width at 6 μm through simulation. To sum up, we successfully selected the optimal ridge width, etching depth and array period parameters through COMSOL.

Before the top cladding layer was grown, a buried 2nd-order grating (period Λ = 1.58 μm, duty cycle σ = 0.4, and depth d ~ 180 nm) was patterned and transformed on the InGaAs upper constrain layer by using holographic lithography and wet etching technique, as is shown in Fig. 2(a). Then the wafer was etched into a five-element CRW structure through standard photolithography techniques and reactive ion etching (RIE). The etching depth was about 2.8 μm and the top

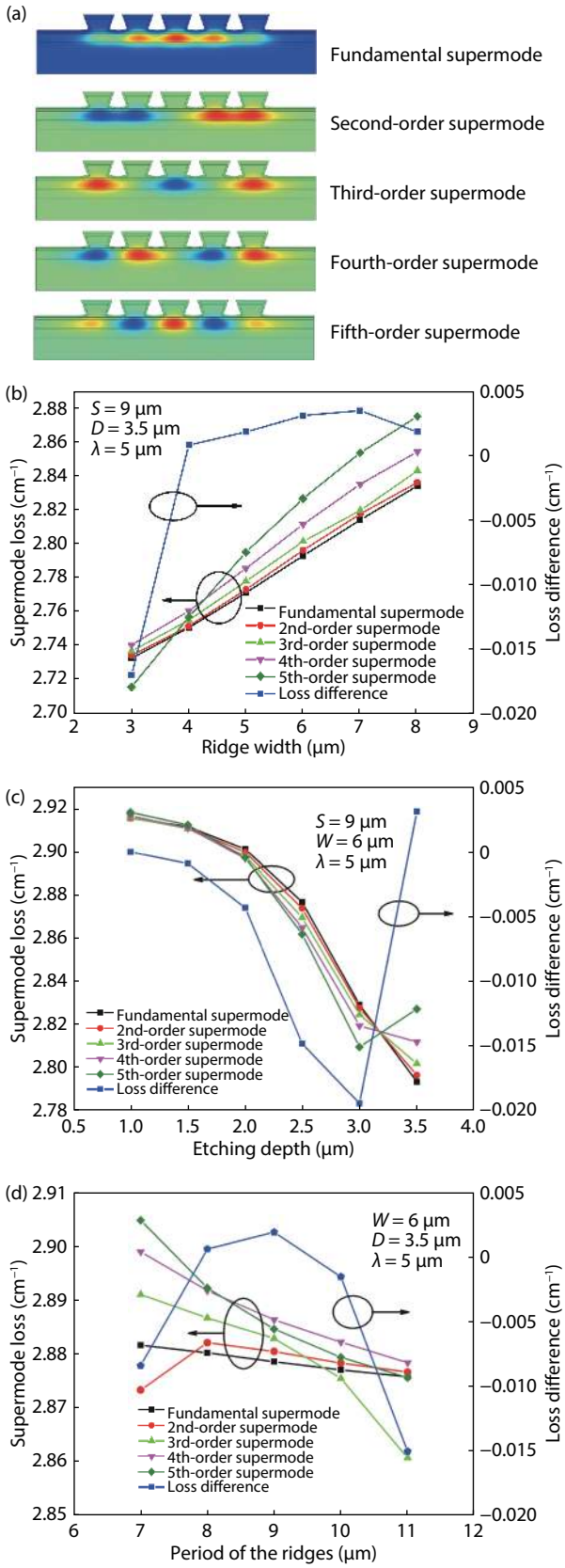

Fig. 1. (Color online) (a) The near-field distribution of the fundamental supermode and high-order supermode. (b) The dependence of loss difference of the modal waveguide between the high-order and fundamental supermode on ridge width with a fixed etching depth at 3.5 μm and array period 9 μm. (c) The dependence of loss difference on the etching depth with a fixed ridge width at 6 μm and period of array at 9 μm. (d) The dependence of loss difference on period of array with a fixed ridge width at 6 μm and etching depth at 3.5 μm.

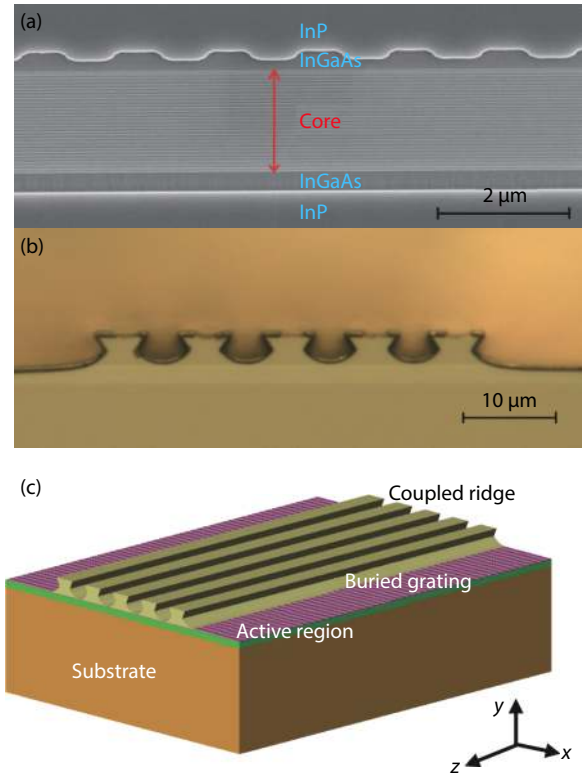

Fig. 2. (Color online) (a) The image of the buried grating from SEM. (b) The cross-section photography of the device. (c) A 3-D sketch of the structure.

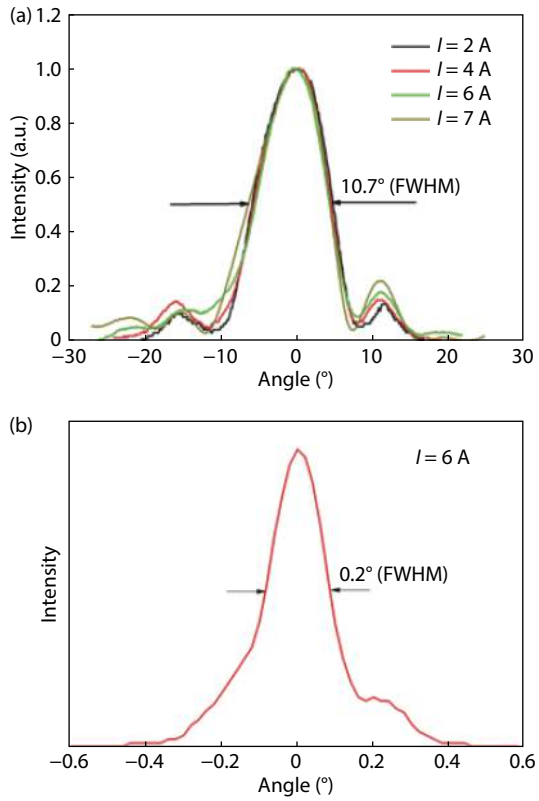

Fig. 3. (Color online) (a) The devices' far-field distribution from the substrate emitting windows in the ridge-width direction at different operating current. (b) The far-field distribution from the substrate emitting windows of the QCL array in the cavity direction at the current of 6 A.

ridge width was 7 μm. This was the first etching step and a good etching profile was ensured by the excellent isotropy of RIE. After that, a wet chemical etching process was used to enlarge the etching depth. Then an inverted conical geometric structure can be obtained, where there is a larger index contrast between the etched and un-etched regions. A total etching depth of 3.5 μm was obtained, which means that we protected the integrity of the active region. Due to the isotropy of the wet etching, the top ridge width was decreased from 7 to 6 μm. The interelement space between two adjacent ridges was 3 μm. The cross-section image of the five-element device was shown as Fig. 2(b). Through this two-step etching method, the loss difference was increased considerably and the coupling strength among array elements was enhanced for mid-wave infrared QCL arrays.

After completing the etching process, a SiO_2 insulating layer with a 450 nm thickness was deposited by plasma-enhanced chemical vapor deposition (PECVD) around the ridges. We set a 3 μm wide window for electron injection on each ridge by photolithography and wet etching and ohmic contact was provided by a Ti/Au layer. To further enhance the heat dissipation, an additional 4 μm thick gold layer was electroplated. Then we deposited a Ge/Au/Ni/Au metal contact layer on the backside of the sample after thinning the substrate down to 150 μm. And then a 160 μm wide substrate-emitting window was patterned by chemical etching. Finally, the sample was high-reflectivity (HR) coated with Al_2O_3/Ti/Au/Al_2O_3 (200/10/100/120 nm) on the back facets by e-beam evaporation, and then cleaved into 2 mm long devices for testing. The QCL arrays were bonded epi-layers down to a copper heatsink with an indium solder.

3. Results and discussion

The far-field pattern of the laser arrays in the ridge-width direction was most concerned. QCL arrays' far-field measurements were carried out on a step-motor controlled rotation stage with a thermal resistor and a thermo-electrical cooler (TEC) monitoring and regulating the heatsink temperature. The devices were operated under a pulsed mode at 25 °C with a repeat frequency of 10 kHz and a pulse width of 1 μs. The mid-infrared emission was collected by a room-temperature HgCdTe detector (Viggo, PVMI-8) with a distance of 40 cm away from the substrate-emitting window of the laser array. For the substrate emitting device, a main-lobed far-field distribution with a divergence angle of 10° was observed in the ridge-width direction at 2 A, as shown in Fig. 3(a). The full width at half maximum (FWHM) of the far-field main-lobes were about 1.5 times the diffraction limit (D.L.) near the threshold. The devices did not operate in single-spatial mode causing the nearest-neighbor coupling to be inevitable due to a very low loss differential. In addition, the inevitable nearest-neighbor coupling may lead to other modes and different modes have different thresholds. Then, while the current increased from the threshold, other modes occurred, the far-field would widen and other peak intensities become obvious. But even at a high current of 7 A, the devices still kept the main-lobed far-field distribution with a divergence angle of 10.7°. The phenomenon can be concluded from the same equation:

$$D\sin\theta = \pm(k + \delta/2\pi)\lambda,$$

where $\delta = \pi/2$ and the calculated side mode positions (about

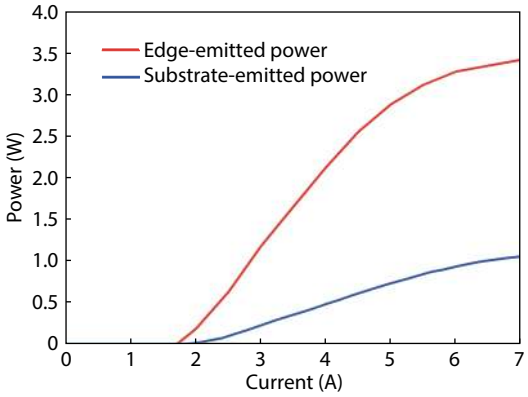

Fig. 4. (Color online) The power–current characteristics of the device at 25 °C. The red line and blue line represent the output power from the edge and the substrate, respectively.

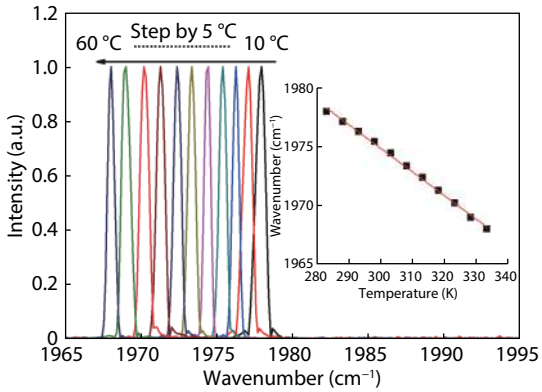

Fig. 5. (Color online) The emitting spectra of the QCL array at different temperatures of the heatsink. The inset shows the dependence of wavelength on heatsink temperature.

16°) correspond to the measured far-field graph. The strong coherent capability of this CRW structure promised a high beam quality, which was very helpful in collimation and long-distance transmission. However, the fundamental transverse mode operation can be only maintained in several number of ridges still due to poor mode discrimination, thus the maximum active ridge width is about dozens of microns. But this structure still makes sense in order to increase the peak power to a certain level. When the laser was measured as an edge emitting device, the far-field displayed a similar phenomenon. In addition, another advantage of this approach is that there is no increase in waveguide loss. Different from the surface semiconductor/Au grating structure, the lowest threshold gain mode in a buried 2nd-order semiconductor/semiconductor grating structure is the symmetric mode[17]. Here we could observe a single-lobed pattern with a small beam divergence of 0.2° near the diffraction limit in the cavity-length direction.

The power–current characteristics of the laser arrays are shown in Fig. 4. The test was carried out at room temperature of 25 °C in the pulsed mode with a repeated frequency of 10 kHz and pulse width of 500 ns. The emitted light power was measured by a calibrated thermopile detector (Coherent, EMP1000) placed directly ahead of the device. For the five-element device, the threshold current was about 2 A and the corresponding threshold current intensity was about 2 kA/cm^2. A peak power of more than 1 W was obtained from the substrate with a slope efficiency of 0.3 W/A. The peak power emitted from the edge was about 3.4 W. The ratio of substrate-emitted power and edge-emitted power was about 31%.

The spectra of the QCL arrays were measured by a Fourier transform infrared (FTIR) spectrometer in a fast scan mode with a resolution of 0.25 cm^{-1}. The temperature of the heatsink was stabilized with a thermo-electrical cooler (TEC). The emitting spectra of the device are shown in Fig. 5. Steady single-mode emission was observed and the lasing wavelength could be tuned continuously. The spectra were measured at different temperatures of the heatsink from 10 to 60 °C with a step of 5 °C, covering a total tuning range of 9.9 cm^{-1}. The inset of Fig. 5 shows the dependence of the lasing frequency on the temperature of the heatsink. A linear tuning coefficient of –0.2 cm^{-1}/K was deduced. The wide tuning range and linear tuning ability make these devices very promising in spectroscopy applications.

4. Conclusion

We have demonstrated high-power single longitudinal mode substrate-emitting QCL arrays lasing at $\lambda \sim 5$ μm by employing a CRW structure and buried 2nd-order DFB grating. Five-element QCL arrays were simulated and fabricated to explore the coherent capability of the CRW structure. Stable main-lobed far-field distribution in the ridge-width direction with a divergence angle of 10.7° was observed even at full power. The peak output power surpassed 1 W at room temperature of 25 °C. The devices could work at a stable single longitudinal mode and could be tuned continuously with a linear temperature tuning coefficient of –0.2 cm^{-1}/K.

Acknowledgements

This work was supported by National Basic Research Program of China (Grant Nos. 2018YFA0209103, 2018YFB2200504), in part by National Natural Science Foundation of China (Grant Nos. 61991430, 61774146, 61790583, 61734006, 61835011, 61674144, 61774150, 61805168), in part by Beijing Municipal Science & Technology Commission (Grant No. Z201100004020006), and in part by the Key projects of the Chinese Academy of Sciences (Grant No. 2018147, Grant No. YJKYYQ20190002, Grant No. QYZDJ-SSW-JSC027, Grant No. XDB43000000, Grant No. ZDKYYQ20200006). The authors would appreciate P. Liang and Y. Hu for their help in the device fabrication processing.

References

[1] Bai Y, Tsao S, Bandyopadhyay N, et al. High power, continuous wave, quantum cascade ring laser. Appl Phys Lett, 2011, 99, 261104

[2] Centeno R, Marchenko D, Mandon J, et al. High power, widely tunable, mode-hop free, continuous wave external cavity quantum cascade laser for multi-species trace gas detection. Appl Phys Lett, 2014, 105, 261907

[3] Slivken S, Sengupta S, Razeghi M. High power continuous operation of a widely tunable quantum cascade laser with an integrated amplifier. Appl Phys Lett, 2015, 107, 251101

[4] Bai Y, Slivken S, Darvish S R, et al. High power broad area quantum cascade lasers. Appl Phys Lett, 2009, 95, 221104

[5] Bai Y, Darvish S R, Slivken S, et al. Electrically pumped photonic crystal distributed feedback quantum cascade lasers. Appl Phys Lett, 2007, 91, 141123

[6] Lu Q Y, Guo W H, Zhang W, et al. Room temperature operation of

photonic-crystal distributed-feedback quantum cascade lasers with single longitudinal and lateral mode performance. Appl Phys Lett, 2010, 96, 051112

[7] Menzel S, Diehl L, Pflügl C, et al. Quantum cascade laser master-oscillator power-amplifier with 15 W output power at 300 K. Opt Express, 2011, 19, 16229

[8] Bai Y, Slivken S, Lu Q Y, et al. Angled cavity broad area quantum cascade lasers. Appl Phys Lett, 2012, 101, 081106

[9] Kirch J D, Chang C C, Boyle C, et al. 5.5 W near-diffraction-limited power from resonant leaky-wave coupled phase-locked arrays of quantum cascade lasers. Appl Phys Lett, 2015, 106, 061113

[10] Wang L, Zhang J C, Jia Z W, et al. Phase-locked array of quantum cascade lasers with an integrated Talbot cavity. Opt Express, 2016, 24, 30275

[11] Meng B, Qiang B, Rodriguez E, et al. Coherent emission from integrated Talbot-cavity quantum cascade lasers. Opt Express, 2017, 25, 3077

[12] Lyakh A, Maulini R, Tsekoun A, et al. Continuous wave operation of buried heterostructure 4.6 μm quantum cascade laser Y-junctions and tree arrays. Opt Express, 2014, 22, 1203

[13] Hoffmann L K, Hurni C A, Schartner S, et al. Wavelength dependent phase locking in quantum cascade laser Y-junctions. Appl Phys Lett, 2008, 92, 061110

[14] Hoffmann L K, Klinkmüller M, Mujagić E, et al. Tree array quantum cascade laser. Opt Express, 2009, 17, 649

[15] Liu Y H, Zhang J C, Yan F L, et al. Coupled ridge waveguide distributed feedback quantum cascade laser arrays. Appl Phys Lett, 2015, 106, 142104

[16] Liu C W, Zhang J C, Jia Z W, et al. Coupled ridge waveguide substrate-emitting DFB quantum cascade laser arrays. IEEE Photonics Technol Lett, 2017, 29, 213

[17] Yao D Y, Zhang J C, Liu F Q, et al. Surface emitting quantum cascade lasers operating in continuous-wave mode above 70 °C at $\lambda \sim 4.6\ \mu$m. Appl Phys Lett, 2013, 103, 041121

Pengchang Yang earned his bachelor's degree in 2018 from the School of Physics, Shandong University, Jinan, China. Now he is an MS student of School of Microelectronics, University of Chinese Academy of Sciences. He is interested in coupled-ridge waveguide structure and beam combining of quantum cascade lasers.

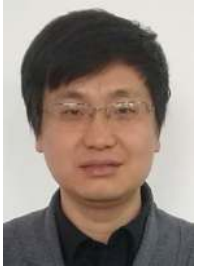

Jinchuan Zhang is an associate professor in the Key Laboratory of Semiconductor Materials Science at the Institute of Semiconductors, Chinese Academy of Sciences. He earned his PhD degree in the Department of electronic engineering at Tsinghua University in 2012. He is interested in designing high-efficiency quantum cascade laser structures, distributed-feedback grating and many others. He is a member of the Youth Promotion Association Chinese Academy of Sciences.

Fengqi Liu is a professor in the Key Laboratory of Semiconductor Materials Science at the Institute of Semiconductors, Chinese Academy of Sciences. He earned his PhD degree in the Department of Physics, Nanjing University, in 1996. Recently, he has demonstrated the quantum dot cascade laser by a two-step strain-compensation active region and material grown technique. He is a winner of the National Outstanding Youth Fund in China.